SHAPE OPTIMIZATION OF COMPRESSOR BLADES USING 3D NAVIER-STOKES FLOW PHYSICS

K. D. Lee*, J. Chung, and J. Shim
Aeronautical and Astronautical Engineering
University of Illinois
Urbana, Illinois 61801

A CFD-based design method for transonic axial compressor blades was developed based on three-dimensional Navier-Stokes flow physics. The method employs a sectional three-dimensional (S3D) analysis concept where the three-dimensional flow analysis is performed on the grid plane of a span station with spanwise flux components held fixed. The S3D analysis produced flow solutions nearly identical to those of three-dimensional analysis, regardless of the initialization of the flow field. The sectional design based on the S3D analysis can include three-dimensional effects of compressor flows and thus overcome the deficiencies associated with the use of quasi-three-dimensional flow physics in conventional sectional design. The S3D design was first used in the inverse mode to find the geometry that produces a specified target pressure distribution. The method was also applied to optimize the adiabatic efficiency of the blade sections of Rotor 37. A new blade was constructed with the optimized sectional geometries at several span stations and its aerodynamic performance was evaluated with three-dimensional analyses.

1. INTRODUCTION

In recent years, a remarkable progress has been made in turbomachinery design methods. The maturation of Navier-Stokes computing technology and the rapid growth in computer capability have led to more reliable and affordable CFD-based design tools. In addition, modern design methods utilizes such design algorithms as inverse design,[1-4] design optimization,[5-9] and neural network[10,11] in order to improve the performance of a blade more systematically and efficiently. Recent research efforts by various groups in developing practical design tools were reviewed and well summarized by Shahpar.[12] Despite the advances in design tools, however, their applications in three-dimensional (3D) designs based on Navier-Stokes physics have been limited due to a large number of flow evaluations required, which is expensive even with today's computing power.

Therefore, a 3D blade is typically constructed by stacking up blade sections at multiple span stations, each of which is designed using a sectional design method. In such designs, the quasi-three-dimensional (Q3D) Navier-Stokes equations are often employed for flow analysis. The purpose of using the Q3D Navier-Stokes equations is to account for some of the 3D effects in turbomachinery flows. For instance, the flow variations in the spanwise direction at a span station can be taken into account by supplying the streamtube geometry as a function of the meridional coordinate, usually obtained with a one-dimensional meridional analysis. For the design of today's high-speed axial compressor blades, however, this type of assumption on the streamtube geometry is unsatisfactory because of substantial spanwise flow components present in the flow field. This Q3D assumption is especially invalid near the end regions of a blade, where the 3D effects are strong. The applications of sectional methods using Q3D flow physics are thus confined to the mid-span regions. Although many sectional design methods have been successfully applied in the past to improve the performance of 3D blades, the authors feel that design results can be improved significantly with a more sophisticated flow modeling that can capture 3D effects in the compressor flow field with higher accuracy.

This paper describes a new design method for the high-speed axial compressor blade based on a sectional three-dimensional (S3D) flow analysis and a numerical optimization. The method is first demonstrated with applications in the inverse design mode and then with design optimizations of blade sections of the NASA Rotor 37 blade to find a new 3D blade with improved performance.

2. SECTIONAL 3D DESIGN

The design process for the developed method is shown schematically in Figure 1. It starts with a 3D flow analysis of an initial blade. Then, for a selected span station, the spanwise flux quantities are stored, and the S3D design is performed on the grid plane at the span station based on the S3D flow analysis. The main design cycle, iterated until overall design criteria are satisfied, consists of five parts: evaluation of objective function, sensitivity analysis, numerical optimization, geometry and grid modification, and S3D

flow analysis. The tools and methods used in each part are described in the following sections.

2.1 Sectional 3D Flow Analysis

The flow analysis of an initial 3D blade was performed using RVC3D,[13] a 3D thin-layer Navier-Stokes flow solver for turbomachinery blades developed by R. Chima. In the analysis, a four-stage Runge-Kutta scheme was used with local time stepping and implicit residual smoothing for faster convergence. The Baldwin-Lomax model[14] was employed for the turbulence modeling. As boundary conditions, the total pressure, total temperature, and absolute inlet flow angle were specified at the inlet plane, the static pressure at the hub of the exit plane, the adiabatic wall condition on blade surfaces, and the periodicity along the outer grid surface, across the wake surface, and inside the tip-clearance region. The solution was considered converged when the average residual was reduced by three orders of magnitude from its initial value and flow quantities converged up to the fourth significant digit.

For S3D analysis, the 3D thin-layer Navier-Stokes equations in the computational coordinates can be rewritten as follows:

$$\frac{\partial q}{\partial t}+J\left(\frac{\partial \hat{E}}{\partial \xi}+\frac{\partial \hat{F}}{\partial \eta}+\overline{G}\right)=\frac{J}{\mathrm{Re}}\left(\frac{\partial \hat{F}_V}{\partial \eta}+\overline{G}_V\right)+H \qquad (1)$$

where

$$q=\begin{pmatrix}\rho\\ \rho u\\ \rho v\\ \rho w\\ e\end{pmatrix} \qquad \hat{E}=\frac{1}{J}\begin{pmatrix}\rho U'\\ \rho uU'+\xi_x p\\ \rho vU'+\xi_y p\\ \rho wU'+\xi_z p\\ eU'+pU\end{pmatrix}$$

$$H=\Omega\begin{pmatrix}0\\ 0\\ -\rho w\\ \rho v\\ 0\end{pmatrix} \qquad \hat{F}=\frac{1}{J}\begin{pmatrix}\rho V'\\ \rho uV'+\eta_x p\\ \rho vV'+\eta_y p\\ \rho wV'+\eta_z p\\ eV'+pV\end{pmatrix}$$

$$\overline{G}=\frac{\partial}{\partial \zeta}\left[\frac{1}{J}\begin{pmatrix}\rho W'\\ \rho uW'+\zeta_x p\\ \rho vW'+\zeta_y p\\ \rho wW'+\zeta_z p\\ eW'+pW\end{pmatrix}\right]$$

$$\hat{F}_V=\frac{\mu}{J}\begin{pmatrix}0\\ F_2\\ F_3\\ F_4\\ F_5\end{pmatrix} \qquad \overline{G}_V=\frac{\partial}{\partial \zeta}\left[\frac{\mu}{J}\begin{pmatrix}0\\ G_2\\ G_3\\ G_4\\ G_5\end{pmatrix}\right] \qquad (2)$$

Detailed formulations of variables in the equations, such as the relative contravariant velocity components (U', V', and W') and the viscous terms, can be found in Reference 13. In Equation (1), $\overline{G}$ and $\overline{G}_V$ are obtained from the initial 3D flow analysis and held fixed in the S3D analysis. Also, after the momentum terms, $\Delta\rho u$, $\Delta\rho v$, and $\Delta\rho w$, are calculated at each time step, their ζ-components are removed to keep the mass flux in the ζ-direction, $\rho W'$, constant.

The S3D flow analysis uses the same solution algorithms and turbulence modeling as the 3D analysis. Similar boundary conditions are specified except that the back pressure at the exit is now fixed with the value obtained from the initial 3D flow solution. The S3D flow analysis starts from the fully converged 3D flow solution at the corresponding span station, so the convergence of exit flow quantities and inlet mass flow rate was monitored to determine the convergence of the flow solution.

2.2 Numerical Optimization and Sensitivity Analysis

The optimization process was driven by DOT,[15] a commercial optimization package built by VMA Engineering. It is based on the constrained optimization method, which requires an objective function to be minimized, F, and, if necessary, constraint functions, g_j's. In general, a constrained optimization problem can be formulated as

$$\begin{aligned}&\text{Minimize:} && F(\vec{X}) && (3)\\ &\text{Subject to:} && g_j(\vec{X})\le 0 && j=1,J\\ & && X_k^L\le X_k\le X_k^U && k=1,K\end{aligned}$$

where $\vec{X}$ is the vector of design variables X_k, J and K are the numbers of constraints and design variables, and superscripts L and U denote the lower and upper limits on design variables, respectively. During the minimization process, search directions and step sizes need to be determined repeatedly to lower the objective function until an optimum is reached. The optimum values of design variables are found when variation of

the Lagrangian, formed by the gradients of the objective and constraint functions, vanishes:

$$\nabla F(\overset{\rho}{X}) + \sum_{j=1}^{J} \lambda_j \nabla g_j(\overset{\rho}{X}) = 0 \qquad (4)$$

where λ_j's are the Lagrange multipliers. Equation (4) is known as the Kuhn-Tucker condition, which is satisfied at any local optimum points. In practice, the design process is terminated when either Kuhn-Tucker condition is reached or the objective and constraint functions remain the same for two consecutive cycles.

During the sensitivity evaluation step, the present study uses the finite differencing technique to obtain the gradients of objective and constraint functions with respect to design variables. For example, the gradient of the objective function is found from

$$\frac{\partial F}{\partial X_k} = \frac{F(\overset{\rho}{X} + \Delta X_k) - F(\overset{\rho}{X})}{\Delta X_k} \qquad (5)$$

Note that, with the finite differencing technique, the sensitivity evaluation for each design variable requires one flow analysis. This implies that the sensitivity analysis performed using only a single CPU will contribute to dramatically increased total design time. Thus, in this study, parallel processing was utilized for the sensitivity analysis in order to speed up the design process and keep the total design time low. With the implementation of Message Passing Interface, the sensitivity evaluations for all design variables were simultaneous carried out using the same number of CPUs as that of design variables.

2.3 Geometry and Grid Modification

A C-type grid was first generated around an initial 3D blade with TCGRID,[16] a 3D grid generator for turbomachinery blades developed by R. Chima. The simple periodicity clearance model[17] was used to model the tip clearance region. A part of the computational domain around NASA Rotor 37 blade is shown in Figure 2. For a S3D design at a span station, the blade sectional geometry and its corresponding grid plane are extracted from the 3D grid at the span station. During the design process, the blade section geometry was modified by adding a linear combination of base functions in the direction normal to the chord line of the blade section. The geometry perturbation, Δn, is defined as

$$\Delta n = \sum_{k=1}^{K} X_k f_k(s) \qquad (6)$$

where $f_k(s)$'s are base functions and s the percent chord. Here, the weighting coefficients, X_k's, are the design variables to be determined through optimization. The base functions used in this study were the Hicks-Henne shape functions[18] without the one specialized for the leading edge and are given as

$$f_k(s) = \sin^3(\pi s^{e(k)}) \qquad (7)$$

where

$$e(k) = \frac{\log(0.5)}{\log(s_k)} \qquad (8)$$

Whenever blade section geometry changed, the field grid points were adjusted accordingly with the linear straining method. A simple elliptic smoothing routine was then applied to ensure the grid quality, but only to the grid points away from the blade surface to retain orthogonality of the grid lines near the surface.

3. VALIDATION OF S3D ANALYSIS

Before the application of the developed design method to design problems, the flow solutions obtained with the S3D analysis were validated against those from a full 3D Navier-Stokes analysis. Blade sections of NASA Rotor 37 blade at 30, 50, and 70 percent span stations were chosen for the comparison of the flow solutions, and the comparisons of the flow solutions revealed excellent agreements between the flow solutions obtained with the S3D and 3D flow analyses, as shown in Table 1 at the 70 percent span station of Rotor 37. The details of this validation result can be found in Reference 19.

4. S3D INVERSE DESIGN

As a validation step, the developed design method was applied in the inverse mode. That is, the S3D design method was applied to find the blade geometry that produces a target pressure distribution. Three tests were performed, using the blade sections of Rotor 37 at 30, 50, and 70 percent span station as target blade geometry and their surface pressure distributions, known from the 3D analysis, as the target distributions. Initial blade sections were produced by adding arbitrary thickness to the target blade profiles. The objective function was chosen as the discrepancy between the target pressure and the pressure of the designed blade section. That is,

$$F = \sum_{i=itl}^{itu} (p_i - p_i')^2 \Delta l_i, \qquad (9)$$

where p_i is the pressure of the designed blade section, p_i' the target pressure, Δl_i the length of the i-th surface segment, and *itl* and *itu* the i-indices for the lower and upper trailing edges, respectively. The grids contained 257 grid points in the streamwise direction with 177 points on the blade surface and 33 points in the blade-to-blade direction. A total of 14 design variables were placed on the blade surface, seven each on pressure and suction sides at 40, 45, 50, 55, 60, 65, and 70 percent chord.

An example is shown in this paper for the case with the blade section at 70 percent span station. Figure 3 (a) shows the geometry of initial blade section, substantially thicker than the target blade geometry. In the figure, the blade section was rotated in order to show more clearly the change in geomery from the design. The design lasted eight cycles, with most of the reduction in the objective function occurring in the first two cycles. Each cycle took on average of about four hours to complete as 14 SGI Origin 2000 processors were used for sensitivity analysis and a single Origin 2000 processor for the remaining parts. The geometry of the designed blade section is compared with that of the target blade section in Figure 3(a), which shows that they are almost identical to each other. The two blade sections also generate nearly identical isentropic Mach distributions on the surface, as shown in Figure 3(b).

5. S3D DESIGN OPTIMIZATION

After the validation stage, the design method was applied to optimize the blade sections of Rotor 37 at 30, 50, and 70 percent span stations. The same grid size and the same number of design variables as in inverse design were used for the design. The design variables were placed on the same chordwise locations as well. The objective function was chosen to improve the adiabatic efficiency of the blade section, in the following form:

$$F = -\frac{\eta}{(\eta)_o} = -\left(1 + \omega_p \Delta p_{o_e} + \omega_T \Delta T_{o_e}\right) \qquad (10)$$

where

$$\eta = \frac{\left(\frac{p_{o_e}}{p_{o_i}}\right)^{\frac{\gamma-1}{\gamma}} - 1}{\frac{T_{o_e}}{T_{o_i}} - 1}$$

and

$$\Delta p_{o_e} = p_{o_e} - (p_{o_e})_o \qquad (11)$$

$$\Delta T_{o_e} = T_{o_e} - (T_{o_e})_o$$

and $(\ )_o$ denotes the value for the initial geometry. The weighting factors ω_p and ω_T are the Jacobians of adiabatic efficiency, η, with respect to the total pressure and total temperature, respectively. In addition, in order to prevent the designed blade section from getting too thin, a constraint on overall blade thickness was imposed as

$$g = 1 - \frac{b_t}{(b_t)_o} \qquad (12)$$

where b_t is the area enclosed by the blade profile.

The optimization for the blade section at 30 percent span station is shown in this abstract. The design was terminated after six design cycles. The design results are summarized in Table 2, which shows that the design improved the adiabatic efficiency of the blade section by about 1.44 percent, mainly attributed to the large gain in exit total pressure. Along with the gain in efficiency, the loss coefficient dropped substantially as well, by about 17.8 percent. The designed blade geometry is compared with the initial geometry in Figure 4(a), where it can be seen that the design caused a slight reduction in camber and a noticeable movement of the point of maximum thickness towards the trailing-edge. As a result of these changes in blade characteristics, the shock strength was reduced, and the shock impingement point on the suction surface was delayed, as shown in Figure 4(b). The amount of delay in the shock impingement point nearly matched the amount of shift in maximum blade thickness, which implies a close relationship between the two. Mach contour plots in Figure 5 further reveal that the design caused the passage shock to become oblique near the suction surface, which means reduced shock strength and the gain in total pressure across the shock. After the shock, the flow accelerates briefly before eventually slowing down, as seen in Figure 5(b).

After S3D design of the blade sections, a 3D rotor blade was constructed. Cubic spline method was used to interpolate the changes in blade geometry along the spanwise direction from those at 30, 50, and 70 percent span stations. The performance of the designed 3D blade was then analyzed using RVC3D code, and its characteristic curves are compared with those of Rotor 37 in Figure 6. The figure shows that the designed blade not only has a much higher efficiency at the design point, but also show better performance over Rotor 37 for a wide range of flow conditions.

6. CONCLUDING REMARKS

The flow field around a transonic compressor blade exhibits highly complex flow features and involves various types of loss phenomena, and hence high-level flow physics is required to produce a reliable flow prediction. In the present design, the three-dimensional Navier-Stokes equations were used for sectional design. Unlike the quasi-three-dimensional flow equations, the present method no longer requires the specification of assumed streamtube geometry and hence can be used for sectional designs beyond the validity of quasi-three-dimensional flow physics. In addition, the present method eliminates the errors from using inconsistent grid geometry and flow solvers between sectional designs and three-dimensional flow analysis. The optimization of Rotor 37 indicates that the present design method can be used to improve the performance of existing rotor blades. The method can be applied to a local region consisted of multiple grid planes and hence can be extended to designs of blade sections near the tip and hub regions of a blade to further enhance the aerodynamic performance.

7. ACKNOWLEDGEMENTS

This research was supported by a grant from the NASA Glenn Research Center with Dr. Eric McFarland as technical administrator. The authors are indebted to Dr. Eric McFarland and Dr. Rodrick Chima for sharing their expertise on turbomachinery. Computations in this work were conducted on SGI Origin 2000 computers at the National Centers for Supercomputing Applications at the University of Illinois at Urbana-Champaign.

8. REFERENCES

1. Tiow, W. T. and Zangeneh, M., "A Three-Dimensional Viscous Transonic Inverse Design Method," ASME Paper 2000-GT-525, 45th International Gas Turbine & Aeroengine Congress & Exhibition, Munich, Germany, May 2000.
2. Damle, S., Dang, T., Stringham, J., and Razinsky, E., "Practical Use of 3D Inverse Method for Compressor Blade Design," ASME Paper 98-GT-115, 43rd International Gas Turbine & Aeroengine Congress & Exhibition, Stockholm, Sweden, June 1998.
3. Wang, Z., Cai, R., Chen, H., and Zhang, D., "A Fully Three-Dimensional Inverse Method for Turbomachinery Blading with Navier-Stokes Equations," ASME Paper 98-GT-126, 43rd International Gas Turbine & Aeroengine Congress & Exhibition, Stockholm, Sweden, June 1998.
4. Demeulenaere, A. and Van den Braembussche, R., "Three-Dimensional Inverse Method for Turbomachinery Blading Design," ASME Paper 96-GT-39, 41st International Gas Turbine & Aeroengine Congress & Exhibition, Birmingham, UK, June 1996.
5. Chung, J., Shim, J., and Lee, K. D , "3D Transonic Compressor Design Optimization with Quasi-3D Flow Physics," FEDSM 00-11075, ASME 2000 Fluids Engineering Division Summer Meeting, Boston, MA, June 2000.
6. Chung, J., Shim, J., and Lee, K. D., "Shape Optimization of Transonic Compressor Blades Using Quasi-3D Flow Physics," ASME Paper 2000-GT-0489, 45th International Gas Turbine & Aeroengine Congress & Exhibition, Munich, Germany, May 2000.
7. Goel, S. and Hajela, P., "Turbine Aerodynamic Design Using Reinforcement Learning Based Optimization," AIAA Paper 98-4774, 7th AIAA/USAF/NASA/ISSMO Symposium on Multidisciplinary Analysis and Optimization, St. Louis, MO, Sept., 1998
8. Brawley S. C. and Hobson, G. V., "Turbine Blade Design Using Parallel Processors," AIAA Paper 96-0452, 34th Aerospace Sciences Meeting and Exhibit, Reno, NV, Jan. 1996.
9. Jennions, I. K. and Stow, P., "A Quasi-Three-Dimensional Turbomachinery Blade Design System: Part II – Computerized System," *Journal of Engineering for Gas Turbines and Power*, Vol. 107, pp. 308 – 316, April 1985.
10. Giannakoglou, K. C., "Designing Turbomachinery Blades Using Evolutionary Methods," ASME Paper 99-GT-181, 44th International Gas Turbine & Aeroengine Congress & Exhibition, Indianapolis, IN, June 1999.
11. Pierret, S. and Van den Braembussche, R., "Turbomachinery Blade Design Using a Navier-Stokes Solver and Artificial Neural Network," ASME Paper 98-GT-4, 43rd International Gas Turbine & Aeroengine Congress & Exhibition, Stockholm, Sweden, June 1998.
12. Shahpar, S., "A Comparative Study of Optimisation Methods for Aerodynamic Design of Turbomachinery Blades," ASME Paper 2000-GT-523, 45th International Gas Turbine & Aeroengine Congress & Exhibition, Munich, Germany, May 2000.
13. Chima, R. V. and Yokota, J. W., "Numerical Analysis of Three-Dimensional Viscous Flows in Turbomachinery," AIAA *Journal*. Vol. 28, No. 5, 1990, pp. 798 – 806.

14. Baldwin, B. S. and Lomax, H., "Thin-Layer Approximation and Algebraic Model for Separated Turbulent Flows," AIAA Paper 78-257, Jan. 1978.
15. Vanderplaats, G. N., *Numerical Optimization Techniques for Engineering Design*, McGraw-Hill Book Company, 1984.
16. Chima, R. V., "Viscous Three-Dimensional Calculations of Transonic Fan Performance," in CFD *Techniques for Propulsion Applications*, AGARD Conference Proceedings No. CP-510, AGARD, Neuilly-Sur-Seine, France, Feb. 1992, pp. 21-1 to 21-19.
17. Chima, R. V., "Calculations of Tip Clearance Effects in a Transonic Compressor Rotor," *Journal of Turbomachinery*, Vol. 120, 1998, pp. 131 – 140.
18. Hicks, R. M. and Henne, P. A., "Wing Design by Numerical Optimization," *AIAA Journal of Aircraft*, Vol. 15, No. 7, 1978, pp. 407 – 412

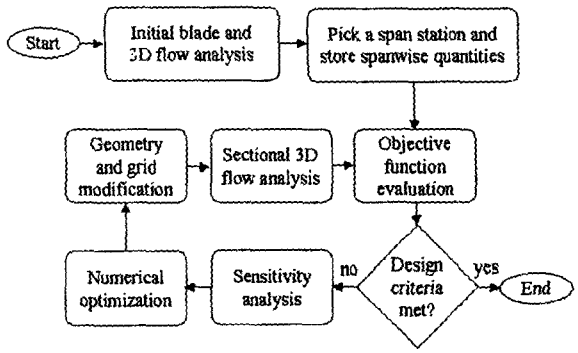

Figure 1. S3D design procedure

Table 1. Comparison of flow characteristics predicted by 3D and S3D flow analyses

	3D	S3D
$(M_{in})_{abs}$	0.56720	0.56751
p_i/p_{oi}	0.80390	0.80371
T_i/T_{oi}	0.93955	0.93948
$(M_{exit})_{abs}$	0.85142	0.85270
p_{oe}/p_{oi}	2.07221	2.07498
T_{oe}/T_{oi}	1.26174	1.26229
η	0.88420	0.88414

Table 2. Design results of optimization

	Initial	Design	Change (%)
η	0.92616	0.93954	1.44467
T_{oe}/T_{oi}	1.26785	1.27070	0.22479
p_{oe}/p_{oi}	2.17207	2.21035	1.76237
c_{loss}	0.15054	0.12378	-17.7760

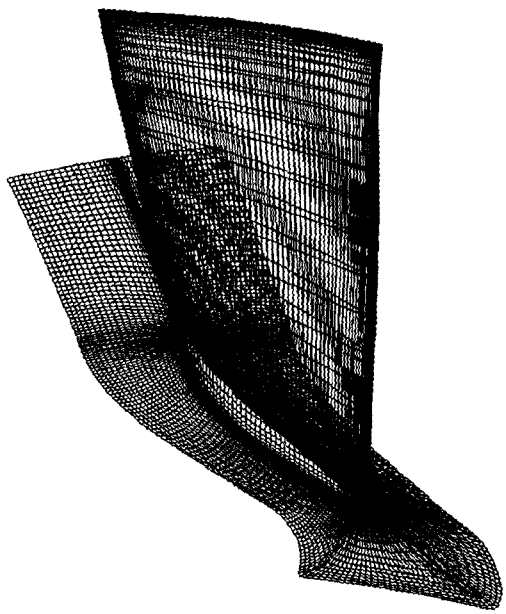

Figure 2. Surface grid of NASA Rotor 37

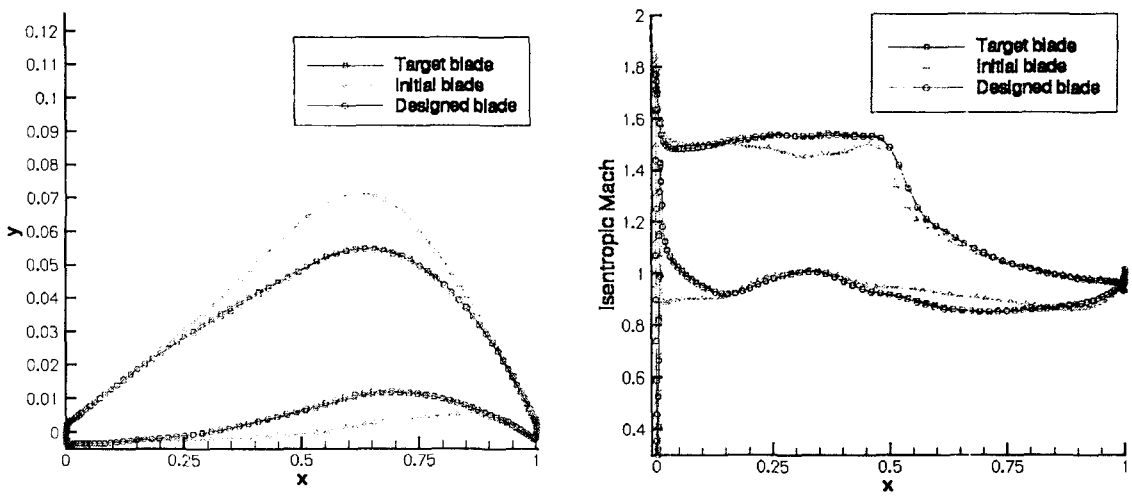

(a) Blade geometry (b) Isentropic Mach distribution

Figure 3. S3D inverse design with blade section of NASA Rotor 37 at 70% span station

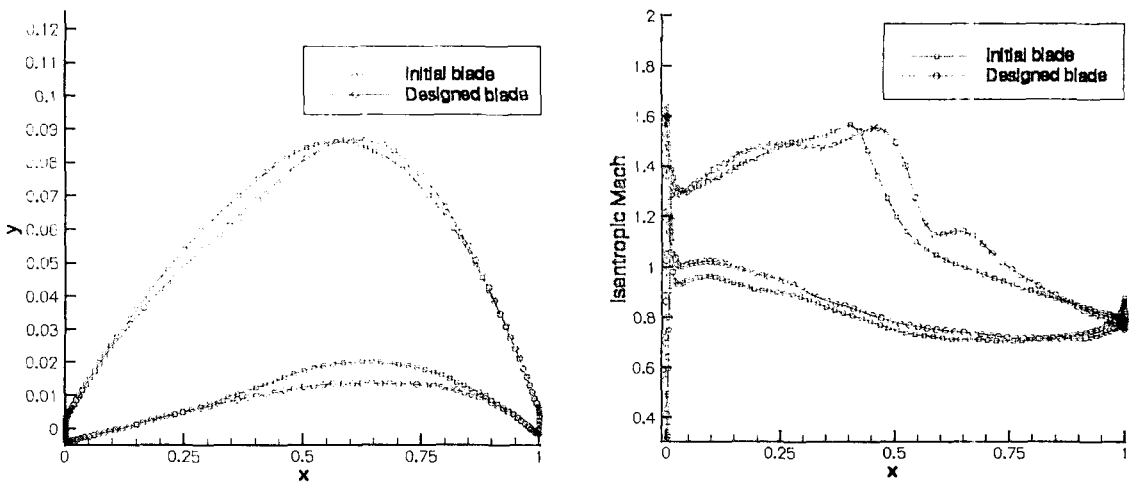

(a) Blade geometry (b) Isentropic Mach distribution

Figure 4. S3D shape optimization on blade section of NASA Rotor 37 at 30% span station

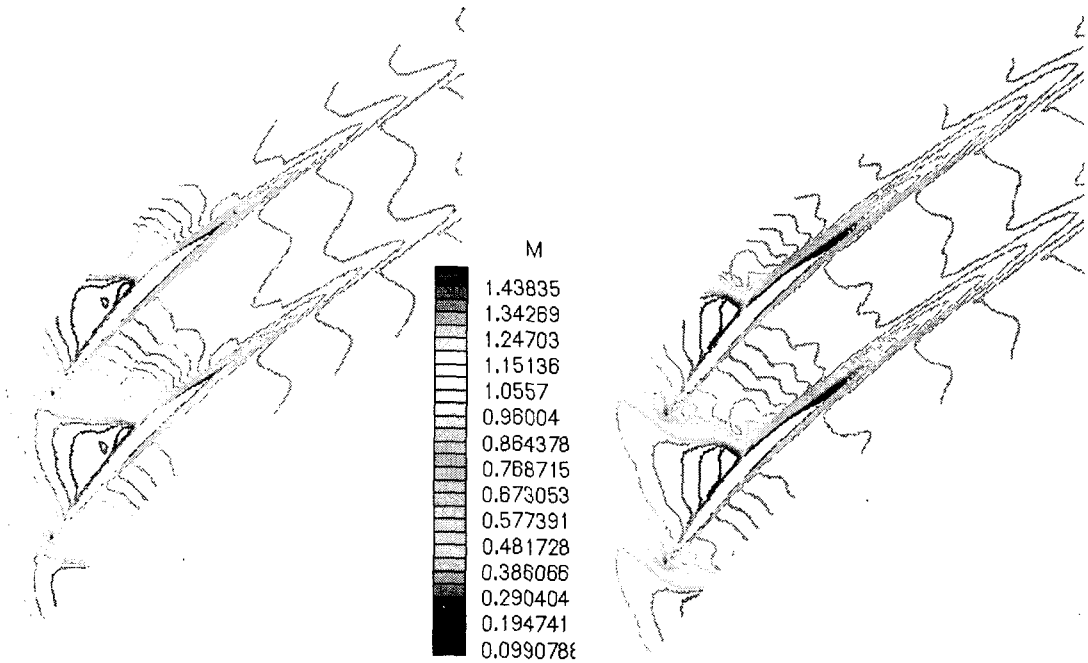

(a) Designed blade section (b) Initial blade section

Figure 5. Mach contours at 30% span station of NASA Rotor 37

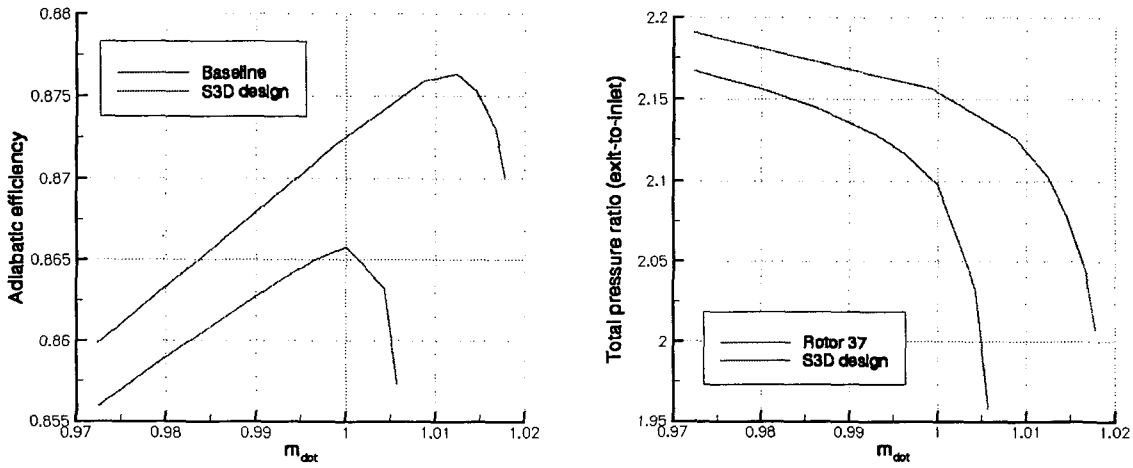

(a) Adiabatic efficiency b) Total pressure ratio

Figure 6. Performance characteristics of NASA Rotor 37 and designed 3D blade